Experimental Characterization of System Parameters for Ranging in IEEE 802.15.4a using Energy Detectors

Bernhard GEIGER[1], *Thomas GIGL*[1,2], *Josef PREISHUBER-PFLUEGL*[2], *Klaus WITRISAL*[1]

[1]Signal Processing and Speech Communication Laboratory, Graz University of Technology, Austria
[2]CISC Semiconductor, Design and Consulting GmbH, Austria

{geiger,thomas.gigl,witrisal}@tugraz.at

Abstract. *The IEEE 802.15.4a standard for impulse radio ultrawide band (IR-UWB) communication systems defines a ranging scheme which relies on the measurement of the round-trip propagation time of electromagnetic pulses. Accuracy is strongly dependent on the estimation of the time-of-arrival (TOA) of the pulse that is spread in time due to multipath propagation. The major concern therefore is the proper detection of the leading edge. In this work, the ranging capabilities of the standard are analyzed for an energy detector receiver. Emphasis is put on the influence of transmitter and receiver parameters, which are evaluated for a set of measured scenarios. It is shown that sub-meter ranging accuracy can be achieved with fixed parameter settings.*

Keywords

Ultrawide band, IEEE 802.15.4a, energy detector, UWB measurements, ranging.

1. Introduction

High temporal resolution, as it is provided by IR-UWB systems, is a prerequisite for accurate ranging. Unfortunately, strict regulations (*cf.* [1]) limit the maximum transmit power level. To cope with subsequently low SNR values, the IEEE 802.15.4a standard defines ternary preamble sequences (TPS) to introduce processing or coding gain [2]. To reduce complexity on the receiver side by keeping the sampling rate low, the energy detector is a receiver architecture widely popular for UWB communication and ranging [3], [4].

Since the detection of the leading edge of the channel response to a transmitted IR-UWB waveform is a fundamental problem in ranging, the majority of the literature focuses on this field without considering coding gain of any kind. Consequently, a multitude of ranging algorithms was developed based on IR-UWB transmission and energy detector reception: from maximum energy selection (MES, [5]) over likelihood based methods [6] to threshold comparison and search-back algorithms (TC, MES-SB, [5], [7]). Threshold selection methods were introduced as well [8], [5], [7], [6], [9], yielding sub-meter ranging in regions with high SNR values.

Some works also analyzed the effects of TPS with perfect cyclic correlation properties which promised to increase ranging performance significantly [9], [10], [11]. Using energy detection receivers unfortunately suffers from non-coherent combining loss, preventing the ranging algorithm from exploiting the full processing gain. Still, sub-meter ranging can be achieved with much lower SNR values due to the usage of TPS. It was also shown that methods developed for ranging with pulses benefit from the transmission of a standard compliant TPS and vice-versa [12].

This work compares ranging algorithms introduced previously in the literature as a function of tunable system parameters, as pulse repetition frequency and length of the TPS code. Receiver parameters such as the integration time and algorithm-specific parameters such as threshold and search-back window size are also evaluated. Moreover, the dependency on channel scenarios – line-of-sight (LOS), office and residential non line-of-sight (NLOS) – is analyzed.

The paper is organized as follows: Section 2 introduces the signal model with emphasis on the TPS defined in the standard, while Section 3 describes the energy detector and a possibility to estimate the power delay profile of the channel from its output. Based on this estimate, Section 4 gives an overview of the ranging algorithms applied in this work. Finally, Section 5 is devoted to the measurement setup for obtaining the channel responses, the simulation settings, and the influence of different ranging parameters.

2. Signal Model

As defined in the IEEE 802.15.4a standard [2], every packet transmission is preceded by a synchronization header (SHR, see Fig. 1) which contains a portion designed for synchronization (SYNC field) and a start-of-frame delimiter (SFD) signaling the end of the SHR.

The SYNC field which is used for ranging purposes consists of N_{pr} repetitions of a preamble symbol, where $N_{pr} \in \{16, 64, 1024, 4096\}$ according to the standard. The

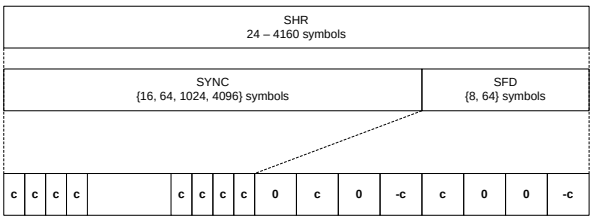

Fig. 1. Synchronisation header structure [2].

preamble symbol itself is obtained by a spreading sequence $\mathbf{c}_s$ built up of ternary elements $\mathbf{c}_s \in \{1, 0, -1\}$, which has perfect cyclic autocorrelation properties [13]. This allows for an easy channel response estimation when coherent receivers are used. However, the most interesting feature of these codes is the fact that even for non-coherent receivers the perfect cyclic correlation properties are preserved, thus making TPS usable for energy detectors as well. Moreover, to maintain performance in multiuser environments, in each channel only a certain set of codes may be used in order to keep cross-correlation between different codes and subsequent multiuser interference at an acceptable level. A low-power way of generating these preamble sequences using linear feedback shift registers was introduced in [10]. The standard defines eight short preamble codes with $N_s = 31$ and 16 long preamble codes with $N_s = 127$ elements (Tab. 1 shows the codes used for the measurements described in Sec. 5.1). The spread preamble code vector is thus created according to the formula

$$\mathbf{c}_{sp} = \mathbf{1}_{N_{pr}} \otimes \mathbf{c}_s \otimes \delta_L = \mathbf{1}_{N_{pr}} \otimes \mathbf{c} \tag{1}$$

where $\mathbf{1}_{N_{pr}}$ is a vector of ones of length N_{pr}, δ_L is the spreading sequence of the preamble, and $\otimes$ denotes the Kronecker product. The spreading sequence δ_L is defined as a unit vector with a one at the first position and length L. Long preamble codes use a spreading length of $L = 4$, whereas short preamble codes can be spread by $L = 16$ or $L = 64$. The latter choice is mainly recommended for environments with a large maximum excess delay τ_{max}.

i	$\mathbf{c}_s$	Channel Nr.
6	++00+00—+-0++-000+0+0-+0+0000	3,6,10,14
13	+000–0000–++0-++++0-0++0+0-00-+0++00 ++-0++0+-+0-00+00-0–000-+-00+0000-0++ -00000+-0-000000-00-+-++-+000-0+0+0+++- 00–00+0+000	0-15

Tab. 1. Ternary codes of the preamble symbols (*cf.* [2]).

The transmitted signal $s(t)$ is obtained by modulation of a train of pulses $w(t)$ with the preamble sequence $\mathbf{c}_{sp}$ and up-conversion to the carrier frequency ω_c:

$$s(t) = \sqrt{\frac{E_p}{N_{pulse}}} \Re \left\{ \sum_{m=0}^{N_c-1} c_m w(t - mT_c) e^{j\omega_c t} \right\} \tag{2}$$

where E_p, N_{pulse}, and $N_c = N_{pr} L N_s$ are the overall energy, the overall number of pulses, and the number of chips in the preamble, respectively. c_m is the m-th element of $\mathbf{c}_{sp}$, and T_c denotes the chip duration. The UWB reference pulse shape $w(t)$ is a root-raised cosine (RRC) filtered pulse with a duration of 2 ns and a roll-off factor of 0.6.

The signal $s(t)$ is then transmitted over the channel, where it is affected by multipath propagation and superimposed with noise. The received signal $r(t)$ thus can be described as

$$r(t) = s(t) * h_c(t) + \nu(t) \tag{3}$$

where $\nu(t)$ is additive white zero-mean Gaussian noise with a two-sided power spectral density of N_0 and the channel impulse response $h_c(t)$ includes the antenna characteristics for simplicity.

3. Energy Detection and Power Delay Profile Estimation

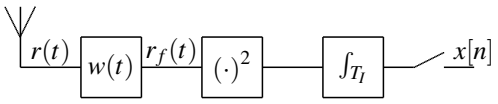

Fig. 2. Energy Detector.

Fig. 2 shows the structure of an energy detector (ED). First, the received signal is filtered by a bandpass filter matched to the pulse shape (i.e. an RRC filter). Next, the filtered signal $r_f(t)$ is squared and integrated over integration periods of T_I, so that the output of the energy detector can be characterized as

$$x[n] = \int_{(n-1)T_I}^{nT_I} r_f^2(t)dt \ . \tag{4}$$

The obtained samples $x[n]$ obviously represent the collected energy between the time instants $(n-1)T_I$ and nT_I. It is noteworthy that some of these samples contain noise energy only, whereas only the minority of samples contain the actual signal. Additionally, the signal energy is distributed over the delay spread of the CIR due to multipath propagation. Assuming that the position of the leading edge is uniformly distributed within the sampling interval T_I, the mean absolute error (MAE) is at least $\frac{T_I}{4}$ if the position of the leading edge is estimated at the center of this interval [5]. Consequently, T_I is limited by receiver complexity and ranging accuracy.

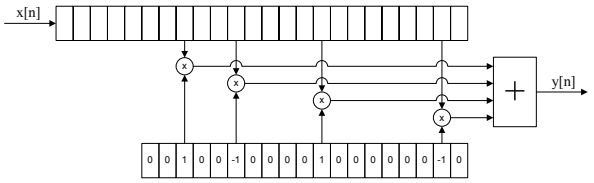

Fig. 3. Sliding window correlator for PDP estimation.

After integration the energy values $x[n]$ are fed into a linear shift register building a part of a sliding correlator (see Fig. 3). The length of the shift register should be equal to the number of energy blocks per preamble symbol, or mathematically

$$N_{reg} = \frac{N_s L T_c}{T_I} \ . \tag{5}$$

The sliding correlator then multiplies the content of the shift register with the reference preamble symbol $\tilde{\mathbf{c}}$, which is obtained by spreading the reference code $\tilde{\mathbf{c}}_s$:

$$\tilde{\mathbf{c}} = \tilde{\mathbf{c}}_s \otimes \delta_{LT_c/T_I} \tag{6}$$

where δ_{LT_c/T_I} is a unit vector with a one at the first position and length $\frac{LT_c}{T_I}$. In order to preserve the perfect cyclic correlation properties, the reference code $\tilde{\mathbf{c}}_s$ has to be constructed based on the preamble code: The preamble code sequence $\mathbf{c}_s$ has to be converted to a binary sequence by taking the absolute value of each code element (so that all active elements are 1) and then setting all non-active elements to -1 [10]. The spread preamble and reference symbols as well as their cross-correlation can be seen in Fig. 4. In [12] a second way of designing $\tilde{\mathbf{c}}_s$ was illustrated. In order to guarantee the reference code to be zero-mean and thus reduce noise accumulation, all non-active code elements have to be set to $-\frac{16}{15}$ (or $-\frac{64}{63}$ for the long preamble codes). As a trade-off one has to sacrifice perfect correlation properties.

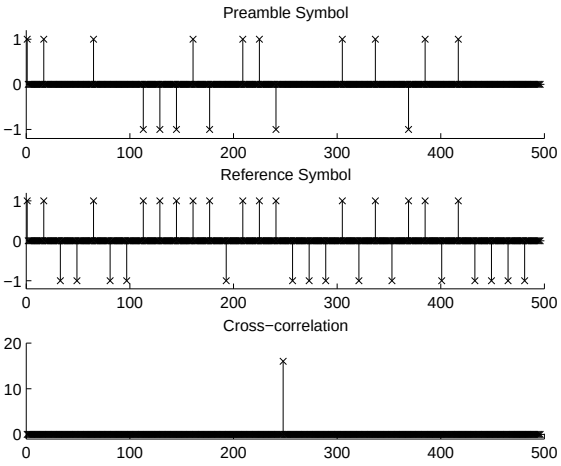

Fig. 4. Cross-correlation for preamble symbol and reference symbol.

The products of the multiplication of the register contents with the reference symbol are then accumulated over N_{pr} symbols in order to further reduce the noise variance relative to the signal energy. This yields a sampled version of the squared, filtered CIR – the power delay profile (PDP) estimate $y[n]$:

$$y[n] = \sum_{q=0}^{N_{pr}-1} \sum_{m=0}^{N_{reg}} \tilde{c}_m x[m-n-qN_{reg}] \tag{7}$$

where $\tilde{c}_m$ is the m-th element of $\tilde{\mathbf{c}}$. For a more detailed description of this correlation process the interested reader should refer to [14]. Due to spreading, the reference symbol is sparse, thus only N_s multiplications are necessary (all other elements are zero). If furthermore $\tilde{\mathbf{c}}_s$ is constructed to achieve perfect cyclic cross-correlation with $\mathbf{c}_s$, all multiplications can be reduced to additions and subtractions (all active elements are 1 or -1).

4. Ranging using TPS

After obtaining a noisy PDP estimate, the leading edge has to be detected for accurate ranging. Since this problem is elemental for ranging, there exists a wide field of literature addressing leading edge detection. However, only few consider the low-complexity approach that is pursued in this work, where a single ED with a fixed integration period T_I is used [6], [5], [15]. This Section gives a brief overview of the algorithms evaluated in the experiments; Maximum energy selection (MES), MES search-back (MES-SB) and MES search-forward (MES-SF) (see Fig. 5).

Maximum energy selection (MES) is the most simplistic and robust way of TOA estimation. From all energy blocks $y[n]$ of the PDP estimate the one with the maximum energy is assumed to contain the leading edge [5]. Mathematically, this can be described by

$$\hat{\tau}_{MES} = \left[\arg\max_n \{y[n]\} + \frac{1}{2}\right] T_I = \left[n_{max} + \frac{1}{2}\right] T_I \tag{8}$$

where n_{max} is the index of the strongest peak and the center of the block is selected as TOA estimate. Depending on the scenario, the leading edge is not identical to the strongest path and consequently big ranging errors are caused.

As a refinement of MES, MES search-back (MES-SB) uses a window of length w_{SB} in front of the strongest peak. In regions with sufficient SNR, it is sensible to assume that the leading edge is either contributing its energy to MES or to an earlier block, so by employing threshold comparison within a search-back window preceding and including the MES block, the ranging accuracy can be increased while keeping the robustness linked to pure MES [5], [7]. The first peak which exceeds the threshold ζ *within this window* is chosen as an estimate for the TOA. Mathematically,

$$\hat{\tau}_{SB} = \left[\min_n \{n | \tilde{y}[n] > \zeta\} + n_{max} - \frac{w_{SB}}{T_I} - \frac{1}{2}\right] T_I \tag{9}$$

where $\tilde{y}[n]$ collects all blocks within the search-back window,

$$\tilde{y}[n] = \left[y[n_{max} - \frac{w_{SB}}{T_I}] \cdots y[n_{max}]\right] \ . \tag{10}$$

In addition to threshold selection, also the size of the search-back window w_{SB} has to be chosen. If the search-back window is chosen too small, it is likely that the leading edge does not contribute to blocks within that window. If it is chosen to large, the probability that noise-only blocks exceed ζ increases.

This probability can be reduced greatly by not choosing the first block exceeding ζ but the last block below ζ, and taking the immediately succeeding block as TOA estimate. This method, called MES search-forward or MES-SF

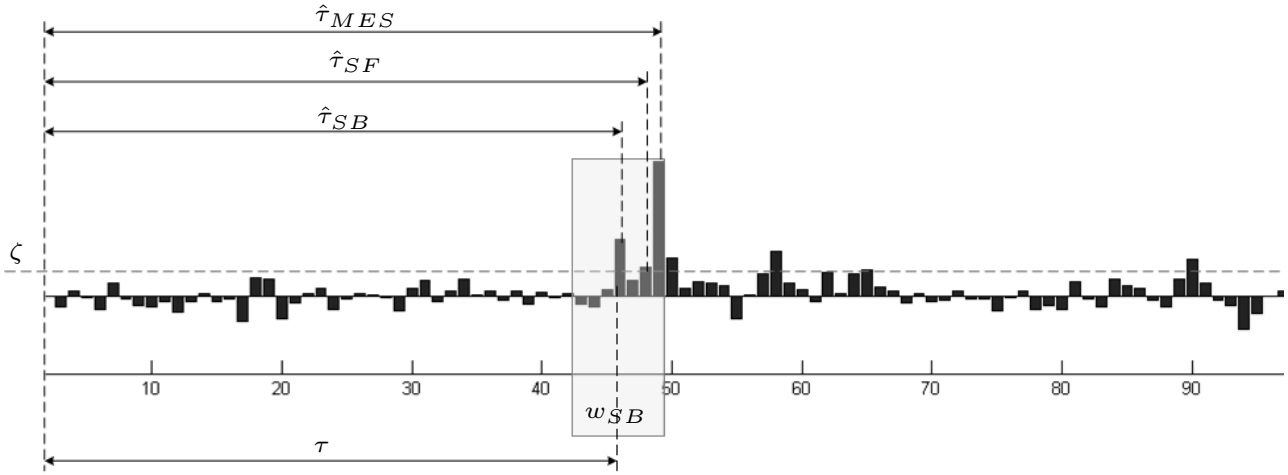

Fig. 5. Different methods of TOA estimation (using TPS).

was introduced in [12], [16] and can be described using the formula

$$\hat{\tau}_{SF} = \left[\max_n \{n|\tilde{y}[n] < \zeta\} + n_{max} - \frac{w_{SB}}{T_I} + \frac{1}{2}\right] T_I \,. \qquad (11)$$

As already mentioned, a threshold has to be chosen for the last two methods depending on signal statistics. In this work, the threshold selection algorithm from [17] was adapted to ranging with TPS. Based on a design parameter ζ_{norm} the threshold ζ is computed according to

$$\zeta = \bar{\eta} + \zeta_{norm}\,(y[n_{max}] - \bar{\eta}) \qquad (12)$$

where $\bar{\eta}$ is the standard deviation of the noise-only portion of the PDP estimate. Although the receiver complexity is slightly increased by making noise estimation necessary, this effort can be justified by the fact that the design parameter ζ_{norm} is now relatively independent of the SNR. By choosing a normalized threshold according to (12), the probability of false alarms due to noise-only blocks is very low. On the other hand, the probability of leading edge misses increases.

5. Experiments and Results

5.1 Channel Measurements

For the ranging experiments a set of channel impulse responses was measured using the UWB demonstrator system introduced in [18]. In this system a field programmable gate array (FPGA) generates preamble sequences, which are up-converted using a vector signal generator after standard compliant pulse shaping. These up-converted pulses are then transmitted over the radio channel using UWB antennas, received, amplified and sampled with a digital oscilloscope. The sampling rate was set to 2 GS/s so that the upconverted pulses were aliased due to undersampling. The preamble symbols were then stored for offline post-processing. Post-processing was done using Matlab, where a coherent receiver was implemented for correlation and averaging so that inter pulse interference (IPI) [14], [19] was not an issue. As a consequence, the output of the coherent receiver was an estimate $h(t)$ of the channel impulse response $h_c(t)$, where pulse shaping at the transmitter, front-end filtering $h_{front}(t)$, and antenna effects were already included:

$$h(t) = h_c(t) * w(t) * h_{front}(t) \,. \qquad (13)$$

Fig. 6 shows the floor plans of four measurement scenarios: line-of-sight in a narrow hallway (LOS), and non-line-of-sight in two offices (OFF) and in a residential environment (RES). The two smaller office environments were combined, so that for each scenario at least seven locations were considered, differently influenced by obstructions, shadowing or strong reflections. At each location a set of 15 measurements was conducted at a 5x3 grid with a spacing of 10 cm in horizontal and vertical direction. This way a proper analysis of small-scale fading effects was possible [20]. For each scenario more than 100 channel responses were available and could be used for ranging simulations.

The scenarios were quite different with respect to the root mean square delay spread τ_{rms}: The residential environment, although NLOS, has the shortest delay spread of only 8 ns, followed by LOS (11.2 ns) and office NLOS (14.6 ns).

5.2 Simulation Settings

A series of simulations was performed based on the measurements described in Sec. 5.1. Each scenario was treated separately to evaluate the performance of different ranging parameters under certain channel conditions. A peak pulse repetition frequency of 500 MHz was employed, lead-

Fig. 6. Floor plans of the measured scenarios. A gray dot indicates the transmitter position, numbered rectangles indicate the receiver locations: (a) LOS, (b) and (c) office NLOS (OFF), and (d) residential NLOS (RES). Floor plans are not to scale.

ing to a chip duration of $T_c = 2$ ns. The carrier frequency was set to 4.4928 GHz, which corresponds to the mandatory channel in the low band (channel 3). After calculating the channel response $h(t)$ according to Sec. 5.1, the responses were normalized to unit energy.

As already mentioned in Tab. 1 two of the codes allowed for channel 3 were used, one short code (code index 6) and one long code (code index 13; this code is only permitted for private ranging [2]). All possible spreading lengths L (4 for long codes, 16 and 64 for short codes) were tested. Since the processing gain introduced by a higher number of symbol repetitions N_{pr} has been widely analyzed in the literature [12], [14], [6] and since this processing gain is independent of the channel characteristics, a deeper analysis of the influence of N_{pr} is omitted here. For computing the threshold according to (12), the noise-only standard deviation $\bar{\eta}$ was calculated from one half of the PDP estimate consisting of noise-only blocks exclusively. Threshold optimization was done for values of E_p/N_0 ranging between 33 and 52 dB. The reference code $\tilde{\mathbf{c}}_s$ was designed to have perfect correlation properties.

The mean absolute error (MAE) was calculated using the following relationship:

$$MAE = \frac{1}{N_{sim}} \sum_{k=0}^{N_{sim}-1} |\tau_k - \hat{\tau}_k| \tag{14}$$

where τ_k is the actual and $\hat{\tau}_k$ the estimated TOA depending on the ranging method, and N_{sim} is the number of simulations for every scenario.

The remainder of this section discusses the experimental results. The first analyses are devoted to receiver parameters, such as search-back window size, threshold, and integration time. Based on the outcome of these simulations, preamble parameters and ranging algorithms were evaluated for a fixed set of receiver parameters.

5.3 Search-back Window

The first goal was to determine the optimum size of the search-back window w_{SB} for different ranging algorithms and scenarios. In the simulations, w_{SB} was varied between 8 and 40 ns in steps of 4 ns.

Fig. 7 shows the influence of w_{SB} on the ranging performance of MES-SF and MES-SB for short codes with short and long spreading lengths. For fair comparison, the optimum threshold ζ_{norm} was chosen for each search-back window size. As it can be seen in Fig. 7, the MES-SF algorithm shows little dependence on the size of w_{SB}, as long as w_{SB} is long enough to cover the time difference between the strongest path and the leading edge (which is zero for LOS). Different behavior can be observed for the MES-SB algorithm: Here, due to IPI, the performance decreases significantly if the search-back window is chosen too long and IPI leads to an early false alarm [14]. By using the long spreading sequences of $L = 64$, this influence can be reduced and shifted to higher values of w_{SB}. For LOS environments, the performance decrease due to IPI is negligible, because the optimum threshold is above the IPI energy level [14]. In low SNR re-

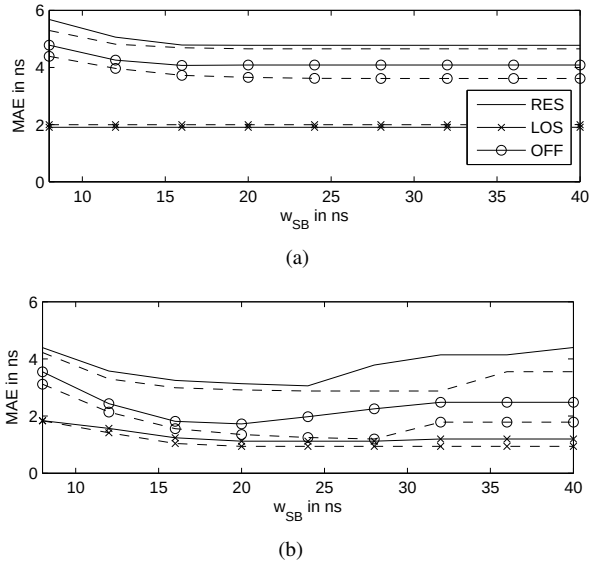

Fig. 7. Influence of w_{SB} on the ranging performance. Spreading parameters $L = 16$ (solid) and $L = 64$ (dashed) were evaluated; $E_p/N_0 = 52$ dB. Optimum ζ_{norm} was chosen for each w_{SB}. (a) MES-SF, (b) MES-SB.

gions, the performance decrease for long windows becomes more and more prominent due to the increased probability of noise-only blocks exceeding the threshold.

For all scenarios and options of ranging parameters (including the ones not depicted in Fig. 7), satisfying results can be obtained by setting the window size to 20 ns. Furthermore, one can see that the ranging accuracy in office NLOS environments is better than in residential NLOS environments. The reason is that for OFF NLOS approx. half of the channel impulse responses have a prominent LOS component despite the fact that the line-of-sight was blocked. Thus, the focus will be put on the RES NLOS scenarios for the remainder of this section.

5.4 Threshold Selection

A proper selection of the threshold design parameter ζ_{norm} is of vital importance for accurate ranging. In the simulations, ζ_{norm} was running between 0.1 and 0.95 in steps of 0.05. In Fig. 8 the influence on the ranging accuracy is analyzed for MES-SF and MES-SB in LOS and NLOS environments. The optimum threshold is both dependent on the amount of noise accumulated and the channel model applying to the actual scenario. As it can be seen in Fig. 8(a) the dependency is much more emphasized for NLOS scenarios, which are in favor of low thresholds. Especially for the MES-SB algorithm the noise has a strong influence, because the increased probability of noise-only blocks exceeding the threshold demands higher values of ζ_{norm}, which in turn lead to high numbers of leading edge misses. Still, for NLOS environments (office and residential) the optimum design parameter turns out to be $\zeta_{norm} = 0.1$.

In LOS scenarios (see Fig. 8(b)) greater thresholds are favorable. One can see that the influence of threshold selection is almost negligible, as long as the threshold is large enough to prevent early leading edge detection due to noise. For MES-SB the optimum threshold is $\zeta_{norm} = 0.35$, for MES-SF it is slightly higher at $\zeta_{norm} = 0.65$, although the influence is even less pronounced there.

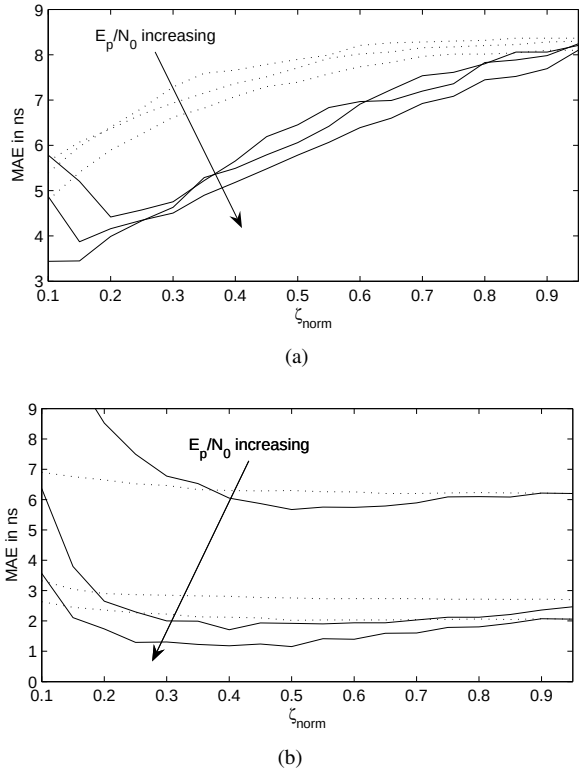

Fig. 8. Influence of ζ_{norm} on ranging performance of MES-SB (solid) and MES-SF (dotted). $T_I = 2$ ns, $w_{SB} = 20$ ns, $L = 16$, and $E_p/N_0 \in \{31, 33, 35\}$. (a) RES NLOS, (b) LOS.

Obviously, for threshold design parameters $\zeta_{norm} = 1$, MES-SB and MES-SF converge to MES, as Fig. 8 verifies.

5.5 Integration Time

The integration period T_I has a strong influence on ranging accuracy in terms of the minimum achievable MAE. Moreover, it can be shown that the choice of T_I influences the probability of proper leading edge detection. Fig. 9 analyzes the performance for different values of T_I for MES-SB and MES-SF. Both LOS and NLOS scenarios were evaluated.

In LOS environments (solid lines), the first arriving path often exceeds all other paths in terms of received energy. However, the combined energy of clusters of reflections may even be greater than that value. As a consequence, integration windows longer than the pulse duration of $T_p = 2$ ns (i.e. $T_I = 4$ ns) lead to a decrease in performance since clustered reflection components and noise get more influence compared to separated LOS components (see Fig. 9). The fact that the theoretical minimum MAE for $T_I = 4$ ns is only 1 ns shows that the performance decrease cannot be related to large integration periods only, but also to im-

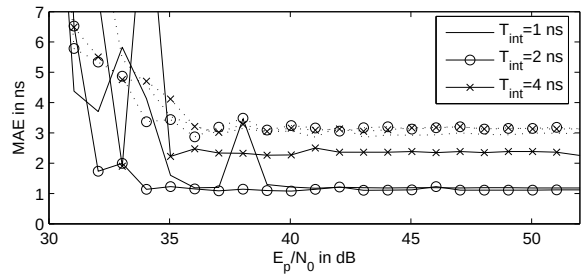

(a)

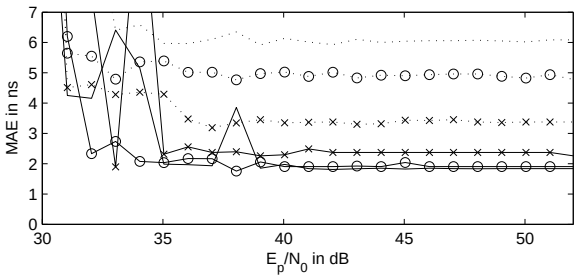

(b)

Fig. 9. Influence of T_I on the ranging performance in LOS (solid) and RES NLOS (dotted) environments. $w_{SB} = 20$ ns, $L = 16$, and design parameter ζ_{norm} according to Sec. 5.4. (a) MES-SB and (b) MES-SF.

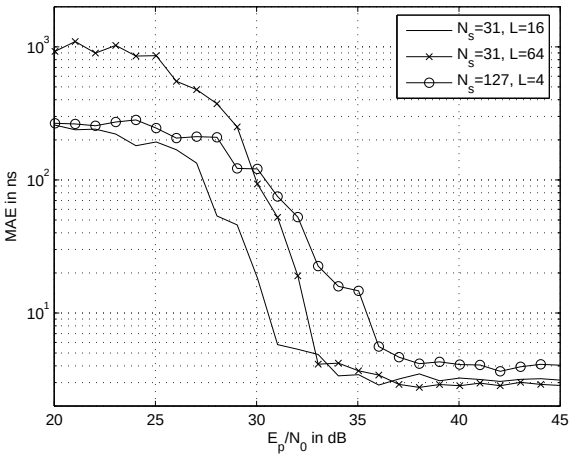

Fig. 10. Analysis of different code and spreading lengths in the RES NLOS scenario. $T_I = 2$ ns, $w_{SB} = 20$ ns, ζ_{norm} according to Sec. 5.4, and $N_{pr} = 16$.

proper leading edge detection. This effect is observable for all ranging algorithms in an LOS environment. Outliers in the plots are explained by mis-detections of MES due to noise peaks.

For MES-SF an interesting phenomenon could be observed: While LOS environments are in favor of short integration periods, for NLOS environments better results could be achieved by increasing T_I as it can be seen in Fig. 9(b). This can be explained by the fact that large integration windows reduce the influence of low-energy portions between the leading edge and the strongest path due to either noise or a large separation between the LOS component and the strongest path.

5.6 Preamble Parameters

To extend the analysis of parameters from the receiver side to the transmitter side, Fig. 10 gives an overview of the properties of the possible parameter settings for signal transmission according to the standard [2] (*cf.* Sec. 2). First, the code length N_s has some influence on ranging with TPS: Using longer codes with $N_s = 127$ and correspondingly shorter spreading lengths of $L = 4$ leads to a higher number of pulses transmitted. Besides the consequently increased transmission energy, such a scheme is also subject to stricter regulations due to an increased duty cycle [1]. As it can be seen in Fig. 10, the long codes suffer from decreased robustness and accuracy if they are compared with respect to overall preamble energy E_p. The long codes increase the preamble energy by 6 dB. Unfortunately, due to non-cohered combining loss, only 3 dB can be exploited for processing gain, so approx. 3 dB more energy is needed to achieve the same output SNR in comparison to the short codes (*cf.* [14]). Reduced accuracy in high SNR regions is related to increased IPI due to the short spreading interval of $L = 4$ (which is equivalent to 8 ns).

Preambles with $N_s = 31$ and $L = 64$ on the other hand show high accuracy in high SNR regions, because IPI has much less effect. The relatively high error in low and medium SNR regions can be explained by the design of the sliding correlator, which performs ranging on the basis of a whole symbol. The uncertainty region is identical to one symbol duration. Thus increasing the symbol length leads to an increased error if due to noise the MES block is uniformly distributed within the symbol [12].

5.7 Ranging Algorithms

Finally, Figs. 11 and 12 compare the ranging algorithms introduced in Sec. 4. As discussed in [5], [6], [12], MES suffers from the fact that in most cases the leading edge does not contribute to the maximum energy block, which explains the relatively high error floor (approx. 8 ns) compared

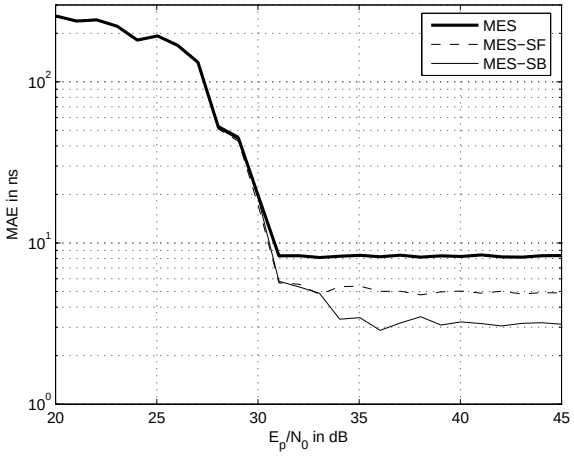

Fig. 11. Comparison of different ranging algorithms (RES NLOS). $T_I = 2$ ns, $w_{SB} = 20$ ns, ζ_{norm} according to Sec. 5.4, and $N_{pr} = 16$.

with more sophisticated algorithms. Naturally, in LOS environments, this excess error is much smaller (approx. 2 ns; see Fig. 12).

MES-SF and MES-SB lead to an improvement in terms of accuracy while linking robustness in medium and low SNR regions to MES [5]. MES-SF does not manage to outperform MES-SB in high SNR regions for $T_I = 2$ ns, but it has the advantage of being widely insensitive to the size of the search-back window w_{SB} and the threshold parameter ζ_{norm}. Moreover, as shown in Fig. 9, MES-SF significantly benefits from larger integration periods, making this approach interesting for low-complexity solutions. For LOS environments, where MES-SB can still yield improvements of approx. 1 ns, MES-SF performs almost identically to MES (see Fig.12).

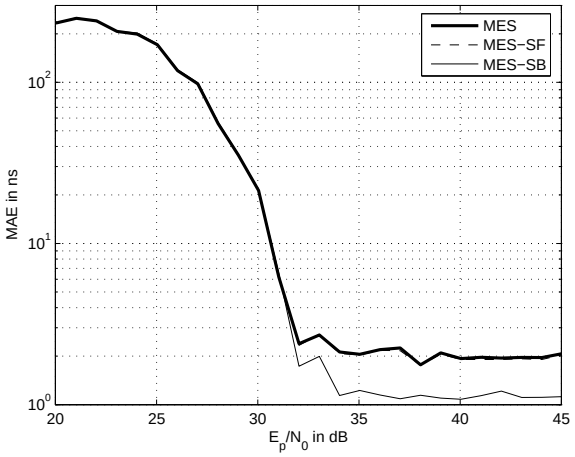

Fig. 12. Comparison of different ranging algorithms (LOS). $T_I = 2$ ns, $w_{SB} = 20$ ns, ζ_{norm} according to Sec. 5.4, and $N_{pr} = 16$.

6. Conclusion

It has been shown, based on a series of simulations with channel measurements of different scenarios, that ranging with ternary preamble sequences is capable of achieving high accuracy while using a single energy detector. Low-complexity threshold-based ranging methods have been introduced and the influence of different ranging parameters on accuracy and robustness has been analyzed. Accuracies close to 3 ns and 1 ns of MAE could be achieved with MES-SB for NLOS and LOS environments, respectively, which translate to sub-meter ranging capabilities if the signal to noise ratio is sufficiently high. It has further been shown that fixed parameter settings can be found that achieve satisfactory results. Hence the complexity for adapting parameter settings online can be avoided.

Acknowledgements

The authors would like to thank Benjamin Till, Graz University of Technology, for his support in conducting the measurements.

References

[1] EUROPEAN COMMISSION. Commission decision of 21 April 2009: On allowing the use of the radio spectrum for equipment using ultra-wideband technology. *Official Journal of the European Union*, L105/9, 2009.

[2] IEEE WORKING GROUP 802.15.4a. *Wireless Medium Access Control (MAC) and Physical Layer (PHY) Specifications for Low-Rate Wireless Personal Area Networks (WPANs): Alternate PHYs*. NJ: IEEE, 2007.

[3] WITRISAL, K., LEUS, G., JANSSEN, G. J. M., PAUSINI, M., TROESCH, F., ZASOWSKI, T., ROMME, J.. Noncoherent ultra-wideband systems. *IEEE Signal Processing Magazine*, 2009, vol. 26, no. 4, p. 48 - 66.

[4] DARDARI, D., CONTI, A., FERNER, U., GIORGETTI, A., WIN, M. Z. Ranging with ultrawide bandwidth signals in multipath environments. *Proceedings of the IEEE*, 2009, vol. 97, no. 2, p. 404 - 426.

[5] GUVENC, I., SAHINOGLU, Z. Threshold-based TOA estimation for impulse radio UWB systems. In *IEEE Int. Conf. on Ultra-Wideband, ICU*. 2005, p. 420 - 425.

[6] GUVENC, I., SAHINOGLU, Z., ORLIK, P. V. TOA estimation for IR-UWB systems with different transceiver types. *IEEE Transactions on Microwave Theory and Techniques*, 2006, vol. 54, no. 4, p. 1876 - 1886.

[7] XU, C., LAW, C. L. Experimental evaluation of UWB ranging performance for correlation and ED receivers in dense multipath environment. In *Future Generation Communication and Networking*. 2007, vol. 2, p. 186 - 192.

[8] GUVENC, I., SAHINOGLU, Z. Threshold selection for UWB TOA estimation based on kurtosis analysis. *IEEE Communications Letters*, 2005, vol. 9, no. 12, p. 1025 - 1027.

[9] LEI, Z., CHIN, F., KWOK, Y.-S. UWB ranging with energy detectors using ternary preamble sequences. In *IEEE Wireless Communications & Networking Conf., WCNC*. 2006, p. 872 - 877.

[10] KWOK, Y.-S., CHIN, F., PENG, X. Ranging mechanism, preamble generation, and performance with IEEE 802.15.4a low-rate low-power UWB systems. In *IEEE Ninth Symposium on Spread Spectrum Techniques and Applications*. 2006, p. 525 - 530.

[11] CHIN, F., ZHI, W., KO, C.-C. System performance of IEEE 802.15.4 low rate wireless PAN using UWB as alternate-PHY layer. In *IEEE Int. Symp. on Personal, Indoor and Mobile Radio Communications, PIMRC*. 2003, p. 487 - 491.

[12] GEIGER, B. Ranging in the IEEE 802.15.4a standard using energy detectors. In *IEEE EUROCON*. St. Petersburg, 2009, p. 1948 - 1955.

[13] SAHINOGLU, Z., GEZICI, S. Ranging in the IEEE 802.15.4a standard. In *Wireless and Microwave Technology Conf.* 2006, p. 1 - 5.

[14] GIGL, T., PREISHUBER-PFLUEGL, J., WITRISAL, K. Statistical analysis of a UWB energy detector for ranging in IEEE 802.15.4a. In *IEEE Int. Conf. on Ultra-Wideband, ICUWB*. Vancover (Canada), 2009, in press.

[15] GUVENC, I., SAHINOGLU, Z. Multiscale energy products for TOA estimation in IR-UWB systems. In *IEEE Global Communications Conf., GLOBECOM*. St. Louis, 2005, p. 209 - 213.

[16] SAHINOGLU, Z., GEZICI, S., GUVENC, I. *Ultra-wideband Positioning Systems – Theoretical Limits, Ranging Algorithms, and Protocols*. Cambridge: Cambridge University Press, 2008.

[17] DIZDAREVIC, V., WITRISAL, K. Statistical UWB range error model for the threshold leading edge detector. In *IEEE Int. Conf. on Information, Communications and Signal Processing, ICICS*. Singapur, 2007, p. 1 - 5.

[18] GIGL, T., BUCHGRABER, T., ADALAN, A., PREISHUBER-PFLUEGL, J., FISCHER, M., WITRISAL, K. UWB channel characterization using IEEE 802.15.4a demonstrator system. In *IEEE Int. Conf. on Ultra-Wideband, ICUWB*. Vancover (Canada), 2009, in press.

[19] GIGL, T., ARNITZ, D., PREISHUBER-PFLUEGL, J., WITRISAL, K. Experimental characterization of ranging in IEEE 802.15.4a using a coherent reference receiver. In *IEEE Int. Symp. on Personal, Indoor and Mobile Radio Communications, PIMRC*. Tokyo (Japan), 2009, in press.

[20] IRAHHAUTEN, Z., JANSSEN, G., HOMAYOUN, N., YAROVOY, A., LIGTHART, L. UWB channel measurements and results for office and industrial environments. In *IEEE Int. Conf. on Ultra-Wideband, ICU*. 2006, p. 225 - 230.

About Authors...

Bernhard GEIGER (S´07) was born in Graz, Austria, in 1984. He finished Higher Technical College in 2003, Graz, and is currently studying Electrical Engineering with focus on Telecommunications at Graz University of Technology. Presently, he is working at his MSc thesis. From 2007 to 2008 he was working as a study assistant at the Institute of Electrical Measurement and Measurement Signal Processing. Since 2007 he is also working as a study assistant at the Signal Processing and Speech Communication Laboratory. His research interests are wireless wide-band and UWB communications, signal processing and free-space optics.

Thomas GIGL was born in Weiz, Austria, in 1979. He finished a higher technical college (HTL) on industrial engineering and management at HTBLA Weiz in 1999 and received the Dipl.-Ing. (MSc) degree in Telematics (Telecommunication and Computer Science) from Graz University of Technology in 2006. In 2006, he wrote his master thesis at Delft University of Technology, The Netherlands. From Jan.-Oct. 2007, he worked as a system and application engineer at CISC Semiconductor, Austria. Since Oct. 2007, he is a PhD student at the Signal Processing and Speech Communication Laboratory (SPSC) of Graz University of Technology. The PhD project is done in cooperation with CISC Semiconductor and focus on low complexity receiver design for UWB positioning systems. His research interests are in signal processing for UWB and wireless communication systems, channel modeling, RFID, RTLS and positioning.

Josef PREISHUBER-PFLUEGL, CTO and Business Unit Manager RFID & RF Comm of CISC Semiconductor Design+Consulting GmbH (www.cisc.at) joined the company in 2003. Starting on 125 kHz reader concepts Josef Preishuber-Pflügl got involved in Radio Frequency Identification (RFID) in 1995 in his master thesis when finishing the Graz University of Technology in Austria with the degree of a Diplomingenieur (Master of Science) in Telematics (Telecommunications and Informatics). He worked in several areas of RFID engineering and product management for system design, reader and tag development covering all frequencies of passive RFID at Philips Semiconductors Gratkorn, Austria. In particular this was the development of a fully integrated 125 kHz reader ASIC based on his demodulator patent, as well as the first worldwide fully integrated 13.56 MHz reader ASIC. In respect to tags he developed several 13.56 MHz ASICs, and full tag designs, before he moved into product management where he led the development of Philips' first UHF product: the UCODE HSL, a tag ASIC according ISO/IEC 18000-4 and ISO/IEC 18000-6. Currently, he is active participant in several standardization groups in the ISO/IEC JTC1/SC31 area, convener of the ISO/IEC JTC1 SC31 WG4/SG6 for RFID performance+conformance, which is responsible for ISO/IEC 18046 and ISO/IEC 18047, and convener of the Austrian standardization group responsible for RFID. Furthermore, he is project editor for the ISO/IEC 18000-6 and did work on the amendment for type C, which is the EPCglobal UHF Class 1 Generation 2 integration into this ISO standard. Since May 2008 he is also vice-chairman of ETSI ERM TG34 for RFID. Under his leadership CISC joined the EPCglobal Inc. in 2004. He is also deeply involved in the EPCglobalTM work. Currently he coves the co-chair positions of SB JRG (Sensor and Battery Joint Requirements Group), HACET (Hardware Action group ad hoc advisory Committee to ETSI) and HAG (Hardware Action Group) representative in the ARC (Architecture Review Committee). Inside CISC he set-up the BU RFID+RFComm with its major activities in modeling, simulation, design, measurement and evaluation of RFID systems and RFID applications for LF, HF and UHF. The major focus in RFID system design is to support product and system design with simulation and measurement tools. This includes a full simulation environment for EPCglobal UHF Class 1 Generation 2 based application considering protocol, identification software and detailed RF aspects.

Klaus WITRISAL received the Dipl.-Ing. degree in electrical engineering from Graz University of Technology, Austria, in 1997, the Ph.D. degree (*cum laude*) from Delft University of Technology, The Netherlands, in 2002, and the Venia Docendi (Habilitation) from Graz University of Technology in 2009. From 1997 till 2001, he was a Ph.D. Student and Research Engineer at Delft University of Technology, in 2002, he was a Project Leader with AVL in Graz, Austria. Currently, he is an Associate Professor at the Signal Processing and Speech Communication Laboratory (SPSC) of Graz University of Technology. His research interests are in signal processing for broadband and UWB wireless communications, propagation channel modeling, and positioning. He is co-chair of the MTT/COM Society of the IEEE Austria Section.